M. WOLLENHAUPT
A. ASSION
O. BAZHAN
D. LIESE
C. SARPE-TUDORAN
T. BAUMERT[✉]

One-parameter control of quantum dynamics using femtosecond pump-probe photoelectron spectroscopy on a model system

Fachbereich Physik, Center for Interdisciplinary Nanostructure Science and Technology, Universität Kassel, Heinrich-Plett-Str. 40, 34132 Kassel, Germany

ABSTRACT Various one-parameter quantum control schemes applied to Na_2 serve as prototypes for current multi-parameter control techniques in order to obtain physical insight into the underlying molecular dynamics.

PACS 31.70.Hq; 33.60.-q; 82.50.Nd

1 Introduction

Microscopic control of the outcome of a chemical reaction is a long-standing dream in physical chemistry. Recently femtosecond lasers have emerged as a particularly suitable tool for quantum control of reaction dynamics. Assion et al. [1] were the first to demonstrate the use of tailored femtosecond laser pulses from a computer-controlled pulse shaper to control the branching ratios of various photodissociation channels in $CpFe(CO)_2Cl$. Moreover, quite recently Levis et al. [2] have suggested that high intensity laser pulses permit to control a dissociative rearrangement reaction in which chemical bonds are not only selectively broken, but also newly formed. Quantum control over chemical reactions may be obtained employing various so-called one-parameter schemes [3–6]. Currently much attention has been focused on the utilization of adaptive feedback controlled femtosecond pulse shaping, which makes available a most versatile instrument for multi-parameter control schemes [1, 7–10]. These techniques have proven to be universal in the sense that they enable to optimize virtually any conceivable quantity and are capable to deliver the optimal electric field without the knowledge of the underlying potential energy surfaces (PES). However, the individual control mechanisms may be inferred, if at all, only for very simple systems. In order to get a better physical insight into the multi-parameter control driving such an experiment, it is essential to investigate one-parameter control schemes in detail on pertinent model systems.

✉ Fax: +49-561/804-4453, E-mail: baumert@physik.uni-kassel.de

2 The sodium dimer as a model system for quantum control schemes

The choice of a suitable model system is governed by several requirements: in order to support the validity of the physical pictures of the control process, full quantum mechanical simulations of the experiment should be feasible. Therefore one-dimensional systems such as diatomic molecules are most workable. Moreover, a detailed knowledge of all PES involved is prerequisite. Insight in the dynamics of the control can only be accomplished if the experiment allows structural and electronic changes in the configuration to be monitored with high spatial and temporal resolution. Measurements of kinetic photoelectrons using time-of-flight spectrometry (TOF) combined with a femtosecond multiphoton ionization pump-probe technique on Na_2 in a molecular beam allows to map molecular motion with sub-Ångström spatial and femtosecond temporal resolution [11]. Therefore these measurements are ideally suited for detailed studies of how quantum control can be achieved. Published and unpublished examples for such one-parameter control schemes elucidating the mechanism of quantum control are presented.

3 The Tannor–Kosloff–Rice scheme

In the time domain, the so-called Tannor–Kosloff–Rice scheme [3] is a very illustrative way of how to obtain control over different products via photoexcitation of a molecule. In practice, a pump laser prepares a vibrational wave packet on an electronic excited potential and a time-delayed probe laser populates the product state either by dumping the wave packet down again or by further excitation. In the case studied here we obtain a higher kinetic energy of the photoelectrons at the inner turning point and a lower kinetic energy of the photoelectrons at the outer turning point from the ionization of a vibrational wave packet propagating on the electronic states (see Fig. 1a for relevant PES and Fig. 1b for measured data). By controlling the duration of the wave packet on the $2\ ^1\Pi_g$ state we have access to different product states (not shown here). By this means we demonstrate the control of the photoproduct ratio Na^+/Na_2^+ in a pump-probe experiment [12].
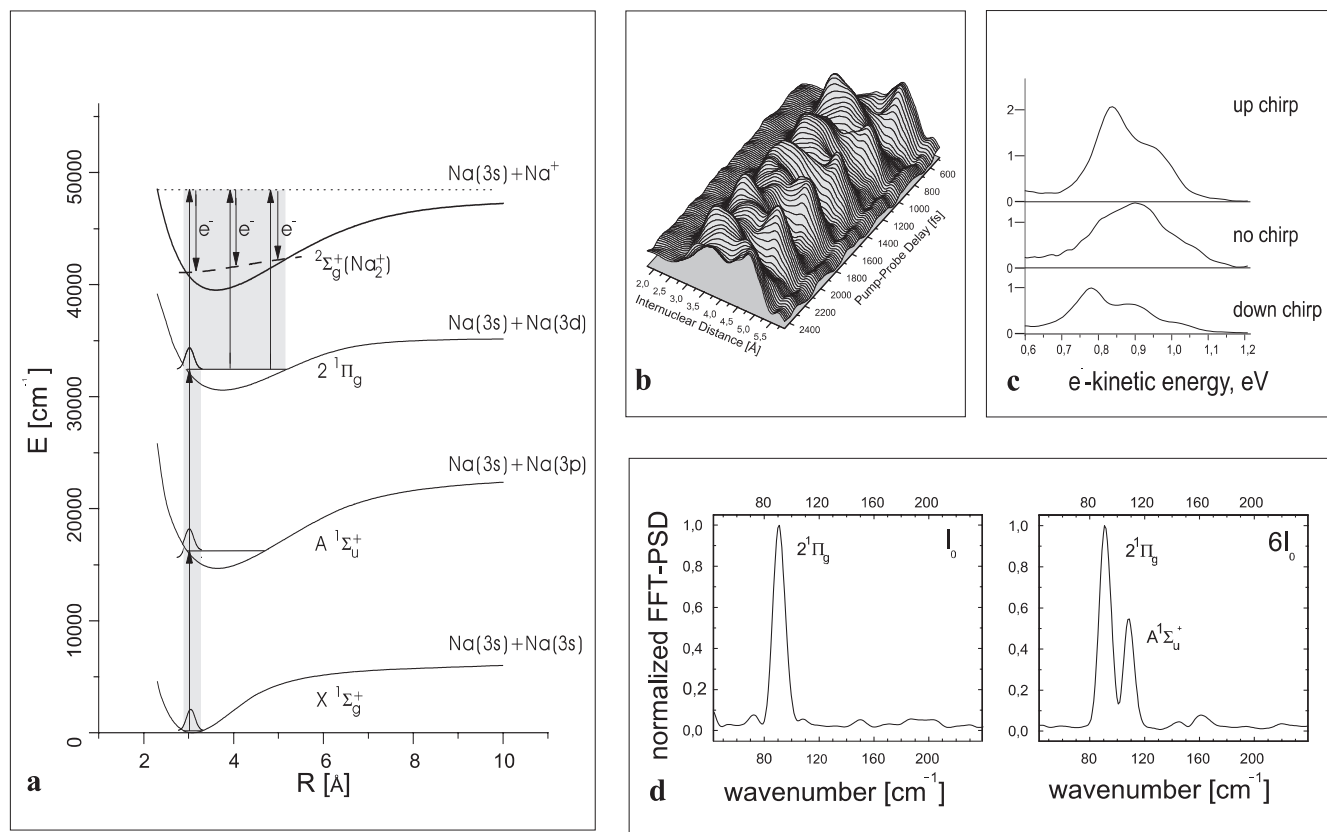
FIGURE 1 **a** Excitation scheme of sodium dimer for 620 nm photons. **b** Mapping the wave packet with sub-Ångström spatial resolution and femtosecond time resolution. **c** Electron spectra measured with single up-chirped ($+3500\,\text{fs}^2$), un-chirped and down-chirped ($-3500\,\text{fs}^2$) laser pulse. **d** Cuts of FFT spectra at the outer turning point of the wave packet at a pump laser intensity of I_0 (*left*) and $6\,I_0$ (*right*)

4   Intensity of the laser pulses

In general, the wavelength range needed for the excitation of an intermediate state will differ from the wavelength range required to reach the product state at a certain bond configuration. If the two wavelength regimes are not contained within the spectral width of the laser pulse, a weak field approach may not be efficient. A solution can be found by utilizing intensity dependent effects. This was demonstrated on Na_2 [13, 14] and also applied in the work of Levis et al. [2]. In a set of measurements the pump laser intensity is kept fixed at $I_0 \approx 10^{11}\,\text{W/cm}^2$ whereas the probe laser intensity is increased from I_0 to $10\,I_0$. The propagation of the vibrational wave packets over all the allowed internuclear distances is monitored with a probe laser of variable intensity to detect the influence of high laser intensities on the molecular potential sensitive to the internuclear distance. In Fig. 1d the FFT (Fast Fourier Transform) of the cuts at TOFs corresponding to the outer turning point of the wave packets are shown. With increasing probe laser intensity a contribution of the A $^1\Sigma_u^+$ state is seen at the outer turning point. An explanation of this resonant behavior is possible in terms of light-induced potentials [13, 15]. The high probe laser intensity also affects the ground state equilibrium position. As seen from the excitation scheme in Fig. 1a, one would expect the frequency contributions of the ground state wave packet at the inner turning point. Figure 2 displays the FFT of TOFs (spectrogram) for a pump intensity of $10^{11}\,\text{W/cm}^2$ and a six times higher probe

intensity (see also Fig. 1d right). Obviously the frequency contributions of the X $^1\Sigma_g^+$ state are shifted to larger internuclear distances. This observation can also be interpreted in the frame of light-induced potentials.

Alternatively the effect of varying the pump laser intensity while keeping the probe laser intensity fixed was also investigated. Figure 3 shows the calculated temporal evolution of
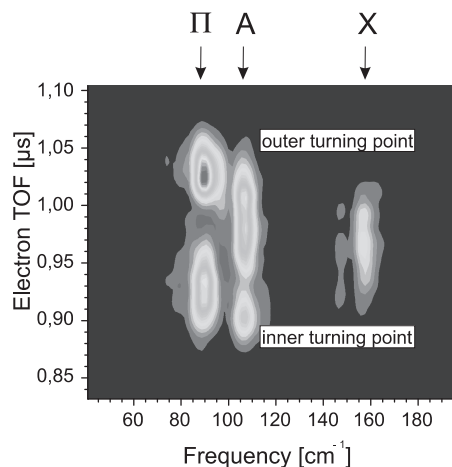

FIGURE 2   FFT of TOFs (spectrogram) for a pump intensity of $10^{11}\,\text{W/cm}^2$ and a six times higher probe intensity. At this probe intensity, in addition to the appearance of the A $^1\Sigma_u^+$ state frequency at the outer turning point, a shift of the ground state frequency to larger internuclear distances is observed
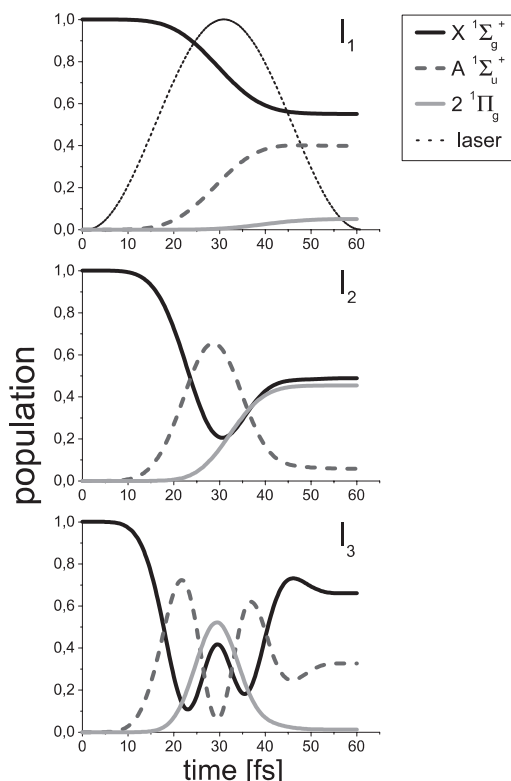
FIGURE 3   Temporal evolution of the population in the X $^1\Sigma_g^+$, A $^1\Sigma_u^+$ and 2 $^1\Pi_g$ states during the pump pulse for laser intensities ranging from $\approx 10^{10}$ to 10^{11} W/cm^2. The laser intensity is drawn as a *dotted line* in the *upper figure*

the population in the X $^1\Sigma_g^+$, A $^1\Sigma_u^+$ and 2 $^1\Pi_g$ states during the pump pulse according to [16, 17]. For low intensities (I_1) the population of the excited states rises monotonously with time. With increasing intensity (I_2) the onset of Rabi oscillation is observed. Population is transferred efficiently within the states during the pump pulse. The highest intensity (I_3) was chosen so that the 2 $^1\Pi_g$ state is completely depopulated at the end of the pump pulse, thereby performing a '2π' excitation. Figure 4 shows the population of the 2 $^1\Pi_g$ state at the end of the pump pulse as a function of the pump intensity. The experimental realization of '2π' excitation is accomplished by increasing the pump laser from I_0 to 2 I_0 and keeping the probe laser intensity at 10 I_0. Figure 5 shows sections through
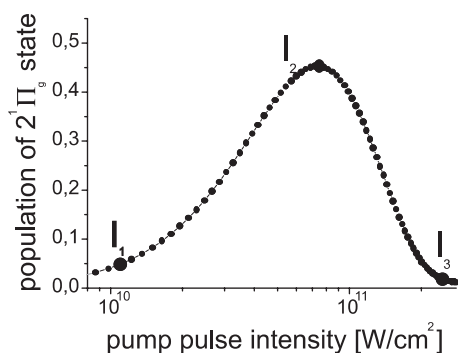

FIGURE 4   Population of the 2 $^1\Pi_g^+$ state at the end of the pump pulse as a function of the laser intensity

the FFT of the photoelectron distribution at the inner turning point for both intensities. At I_0 the contribution at 90 cm^{-1} indicates the presence of population in the 2 $^1\Pi_g$ state. When the pump intensity is doubled the frequency component at 90 cm^{-1} vanishes, thus demonstrating control of the population in the 2 $^1\Pi_g$ state.
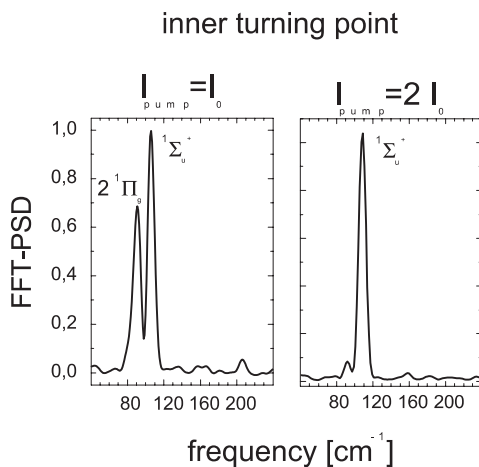

FIGURE 5   Experimental verification of the '2π' excitation; the pulse width is 70 fs, probe intensity = 10 I_0. *Left*: $I_{pump} = I_0 = 10^{11}$ W/cm^2; *right*: $I_{pump} = 2 I_0$

5   Chirp and duration of the laser pulses

In the last couple of years an increasing number of experiments was devoted to the use of phase-shaped laser pulses in order to control atomic and molecular properties [9]. Figure 1c shows photoelectron spectra obtained from ionizing Na$_2$ with up-chirped (3500 fs^2), un-chirped and down-chirped (-3500 fs^2) laser pulses at 620 nm [18]. The pulse intensity is kept below 5×10^9 W/cm^2 and the pulse duration is 40 fs for the transform-limited pulses and 240 fs for the chirped pulses. The ionization yield is seen to double when the frequency order is switched from blue first to red first in the exciting laser pulse. Calculated electron spectra qualitatively reproduce the measured results. From the analysis of these calculations, the importance of synchronizing wave packet motion to chirp and intensity profile for obtaining efficient population transfer is derived.

6   Influence of electronic changes along the internuclear distance

Another aspect in quantum control is introduced by non-adiabatic coupling of the potential curves involved in the time evolution of a quantum system [19]. The coupling of the covalent and ionic potentials in NaI is a prominent example [20, and references therein]. Electronic changes along the internuclear coordinate (R) are also predicted for the $^1\Sigma_u^+$ double minimum potential well in the Na$_2$ molecule (Fig. 6a). According to [21] the change of the electronic structure near the avoided crossing at 4.7 Å leads to photoionization probabilities rapidly changing with geometry. Our approach to measuring the R-dependent photoionization probabilities is based on the comparison of simulated photoelectron spectra
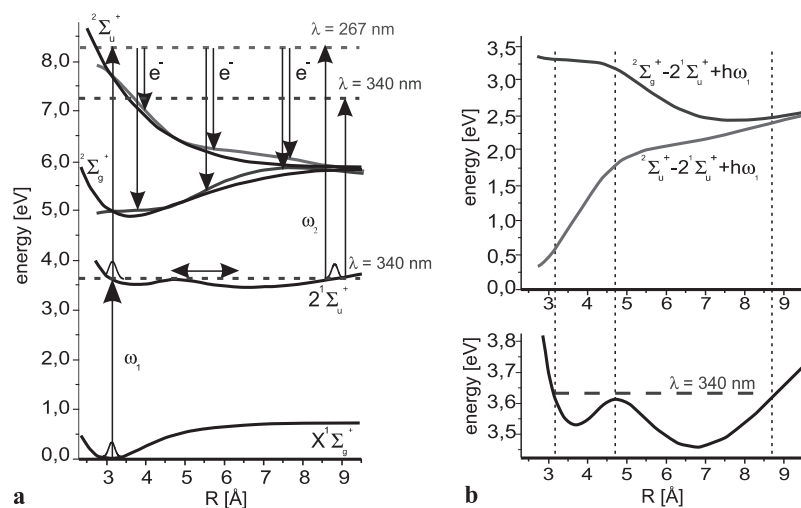
FIGURE 6 **a** Potential scheme of the double minimum of Na_2 for 340 nm photon excitation. The probe wavelength is 267 nm (340 nm). **b** Difference potentials for the ionization into the Na_2^+ $^2\Sigma_g^+$ bound and $^2\Sigma_u^+$ repulsive ionic states at 267 nm

assuming R-independent ionization probabilities and measured data. Moreover the availability of full quantum mechanical calculations including the electronic structure would allow direct comparison of experimental and theoretical results.

In order to investigate the R-dependent ionization probability we simulated a two-color pump-probe experiment on a Na_2 molecular beam using our experimental parameters, i.e. a 40 fs, 340 nm pump and a 267 nm probe laser. The pump laser excites the Na_2 $2\,^1\Sigma_u^+$ double minimum state at the equilibrium position (3.1 Å) of the X $^1\Sigma_g^+$ ($v'' = 0$) ground state at an energy of 3.64 eV slightly above the barrier (3.61 eV) between the inner and outer well (see Fig. 6a for the relevant potential curves). The 5.2 nm bandwidth of the pump laser supports a coherent superposition of vibrational states centered at $v' = 44$ above and below the barrier. The time evolution of the created wave packet is depicted in Fig. 7a. At

150 fs the wave packet reaches the barrier and subsequently bifurcates into a part reflected to the inner well and a transmitted component oscillating within the energetically allowed range of the $2\,^1\Sigma_u^+$ potential of 3 to 9 Å. The oscillation period is seen to be 330 fs and 1 ps in accordance with the corresponding level spacing of 90 cm^{-1} and 32 cm^{-1} for the inner well and the complete potential, respectively. Moreover, at 850 fs the inward moving part of the wave packet starts interfering with the component oscillating within the inner well.

Upon absorption of the probe laser photon Na_2 molecules are ionized to the Na_2^+ $^2\Sigma_g^+$ bound and $^2\Sigma_u^+$ repulsive ionic states. Conservation of total energy and kinetic energy during the ionization process yields the energy of the released photoelectrons. The corresponding difference potentials in Fig. 6b indicate energies of 3.2 and 0.5 eV for photoelectrons emitted at the inner turning point for the bound and repulsive po-
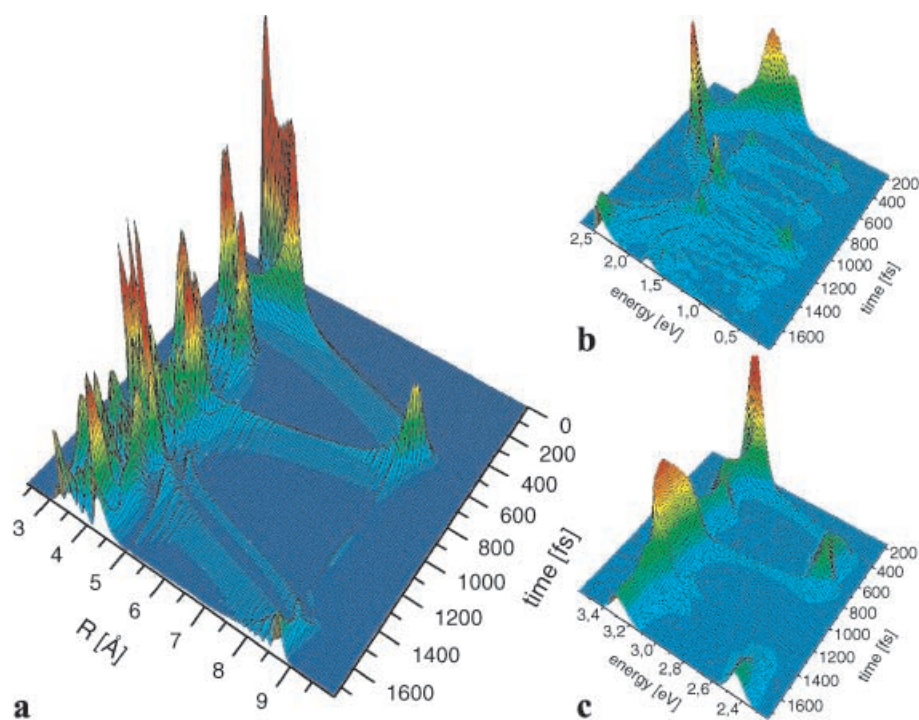

FIGURE 7 **a** Temporal evolution of the wave packet on the Na_2 $2\,^1\Sigma_u^+$ double minimum state excited at the equilibrium position of the X $^1\Sigma_g^+$ ground state at an energy slightly above the barrier. **b** calculated photoelectron signal from ionization into the repulsive ionic state; **c** calculated photoelectron signal from ionization into the bound ionic state

tential, respectively, and 2.5 eV at the outer turning point for both ionic potentials. Generally, the most detailed mapping of the wave packet through the photoelectron distribution is obtained in regions where the difference potentials are steepest. Due to the favorable form of the difference potentials, the complete accessible range of internuclear distances is mapped monotonously onto the energy range of 3.2 to 2.5 eV for the bound curve and onto 0.5 to 2.5 eV for the repulsive potential. The inner (outer) well is imaged with high spatial resolution when photoelectrons from the repulsive (bound) ionic state are observed. The classical difference potential analysis is confirmed by full quantum mechanical calculations (Fig. 7b and 7c) performed analogously to [22] assuming an R-independent ionization probability. From Fig. 7b (photoelectrons from the repulsive ionic state) the high frequency ($90 \, \mathrm{cm}^{-1}$, 330 fs) wave packet motion is clearly seen at photoelectron energies of 0.5 to 1.7 eV. Likewise the slower oscillation with $32 \, \mathrm{cm}^{-1}$ (1 ps) stemming from wave packet components with energies above the barrier is observed most clearly in the energy range from 2.3 to 3.0 eV (bound ionic potential in Fig. 7c).

In the actual experiment Na atoms are present in the Na_2 molecular beam. At our wavelengths Na atoms may concomitantly be excited, i.e. due to near resonance transitions at the pump wavelength ($3s$–$4p$) and at the probe wavelength ($3s$–$6p$) two-photon ionization gives rise to photoelectron signals at 2.2 and 4.2 eV, respectively. Moreover, a pump-probe delay dependent two-color signal at 3.1 eV through pump photon absorption and probe photon ionization is expected due to the ten times stronger dipole moment in favor of the $3s$–$4p$ transition. From these considerations, interference-free Na_2 signals are expected for slow electrons ejected at the inner turning point on the repulsive ionic potential and also for electrons at 2.5 eV released at the outer turning point on both potentials if sufficient energy resolution of the time-of-flight spectrometer is provided.

Preliminary results obtained at the University of Würzburg in a 340 nm one-color pump-probe experiment are depicted in Fig. 8. The Fourier plot shows a distinct maximum at $33 \, \mathrm{cm}^{-1}$ at the outer turning point corresponding to the vibrational period of the transmitted part of the wave packet of about 1 ps. Experiments using a 267 nm probe laser are currently performed which permit to map the complete range of en-
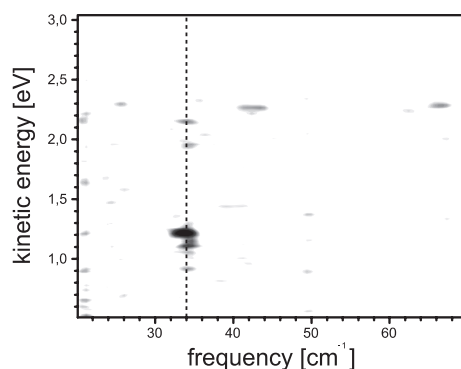
ergetically allowed internuclear distances via the Na_2^+ $^2\Sigma_g^+$ bound and $^2\Sigma_u^+$ repulsive ionic states (Fig. 6a).

7   Conclusion

Investigation of the wave packet motion of small molecules with high spatial and temporal resolution is the key feature to study a variety of one-parameter control schemes in great detail. Several one-parameter control schemes on the model system Na_2 were demonstrated such as the Tannor–Kosloff–Rice scheme, the laser intensity, the chirp and pulse duration and electronic changes along the internuclear distance. Based on this knowledge a comparison to results of feedback optimized laser pulses applied to such systems will provide valuable insights into automated multi-parameter control schemes. Going to larger model molecules, control schemes on isomerization, energy redistribution and molecular rearrangement can be studied using this method because of its sensitivity both to structural and electronic changes in a molecule upon excitation [23].

REFERENCES

1 A. Assion, T. Baumert, M. Bergt, T. Brixner, B. Kiefer, V. Seyfried, M. Strehle, G. Gerber: Science **282**, 919 (1998)
2 R.J. Levis, G.M. Menkir, H. Rabitz: Science **292**, 709 (2001)
3 D.J. Tannor, R. Kosloff, S.A. Rice: J. Chem. Phys. **85**, 5805 (1986)
4 P. Brumer, M. Shapiro: Chem. Phys. Lett. **126**, 541 (1986)
5 U. Gaubatz, P. Rudecki, M. Becker, S. Schiemann, M. Külz, K. Bergmann: Chem. Phys. Lett. **149**, 463 (1988)
6 C.J. Bardeen, Q. Wang, C.V. Shank: Phys. Rev. Lett. **75**, 3410 (1995)
7 R.S. Judson, H. Rabitz: Phys. Rev. Lett. **68**, 1500 (1992)
8 D. Meshulach, Y. Silberberg: Nature **396**, 239 (1998)
9 C.J. Bardeen, V.V. Yakovlev, K.R. Wilson, S.D. Carpenter, P.M. Weber, W.S. Warren: Chem. Phys. Lett. **280**, 151 (1997)
10 T. Hornung, R. Meier, D. Zeidler, K.-L. Kompa, D. Proch, M. Motzkus: Appl. Phys. B **71**, 277 (2000)
11 A. Assion, M. Geisler, J. Helbing, V. Seyfried, T. Baumert: Phys. Rev. A **54**, R4605 (1996)
12 T. Baumert, M. Grosser, R. Thalweiser, G. Gerber: Phys. Rev. Lett. **67**, 3753 (1991)
13 T. Frohnmeyer, M. Hofmann, M. Strehle, T. Baumert: Chem. Phys. Lett. **312**, 447 (1999)
14 T. Frohnmeyer, T. Baumert: Appl. Phys. B **71**, 259 (2000)
15 M. Machholm, A. Suzor-Weiner: J. Chem. Phys. **105**, 971 (1996)
16 C. Meier, V. Engel: *Femtosecond Chem.*, ed. by J. Manz, L. Wöste (VCH, Weinheim 1995) p. 369
17 T. Baumert, V. Engel, C. Meier, G. Gerber: Chem. Phys. Lett. **200**, 488 (1992)
18 A. Assion, T. Baumert, J. Helbing, V. Seyfried, G. Gerber: Chem. Phys. Lett. **259**, 488 (1996)
19 V. Blanchet, M.Z. Zgierski, A. Stolow: J. Chem. Phys. **114**, 1194 (2001)
20 P. Cong, G. Roberts, J.L. Herek, A. Mohktari, A.H. Zewail: J. Phys. Chem. **100**, 7832 (1996)
21 K. Takatsuka, Y. Arasaki, K. Wang, V. McKoy: Faraday Discuss. **115**, 1 (2000)
22 C. Meier, V. Engel: J. Chem. Phys. **101**, 2673 (1994)
23 P. Farmanara, V. Stert, H.-H. Ritze, W. Radloff, I.V. Hertel: J. Chem. Phys. **115**, 277 (2001)

FIGURE 8   Preliminary experimental result: FFT from the measured photoelectron signal at a probe wavelength of 340 nm